JOURNAL OF GEOPHYSICAL RESEARCH, VOL. 115, D09204, doi:10.1029/2009JD013195, 2010

Investigation of cloud condensation nuclei properties and droplet growth kinetics of the water-soluble aerosol fraction in Mexico City

Luz T. Padró,[1] Daniel Tkacik,[2,3] Terry Lathem,[2] Chris J. Hennigan,[3,4] Amy P. Sullivan,[2,5] Rodney J. Weber,[2] L. Greg Huey,[2] and Athanasios Nenes[1,2]

Received 12 September 2009; revised 20 December 2009; accepted 28 December 2009; published 11 May 2010.

[1] We present hygroscopic and cloud condensation nuclei (CCN) relevant properties of the water-soluble fraction of Mexico City aerosol collected upon filters during the 2006 Megacity Initiative: Local and Global Research Observations (MILAGRO) campaign. Application of κ-Köhler theory to the observed CCN activity gave a fairly constant hygroscopicity parameter ($\kappa = 0.28 \pm 0.06$) regardless of location and organic fraction. Köhler theory analysis was used to understand this invariance by separating the molar volume and surfactant contributions to the CCN activity. Organics were found to depress surface tension (10–15%) from that of pure water. Daytime samples exhibited lower molar mass (~200 amu) and surface tension depression than nighttime samples (~400 amu); this is consistent with fresh hygroscopic secondary organic aerosol (SOA) condensing onto particles during peak photochemical hours, subsequently aging during nighttime periods of high relative humidity. Changes in surface tension partially compensate for shifts in average molar volume to give the constant hygroscopicity observed, which implies the amount (volume fraction) of soluble material in the parent aerosol is the key composition parameter required for CCN predictions. This finding, if applicable elsewhere, may explain why CCN predictions are often found to be insensitive to assumptions of chemical composition and provides a very simple way to parameterize organic hygroscopicity in atmospheric models (i.e., $\kappa_{org} = 0.28\varepsilon_{WSOC}$). Special care should be given, however, to surface tension depression from organic surfactants, as its nonlinear dependence with organic fraction may introduce biases in observed (and predicted) hygroscopicity. Finally, threshold droplet growth analysis suggests the water-soluble organics do not affect activation kinetics.

Citation: Padró, L. T., D. Tkacik, T. Lathem, C. J. Hennigan, A. P. Sullivan, R. J. Weber, L. G. Huey, and A. Nenes (2010), Investigation of cloud condensation nuclei properties and droplet growth kinetics of the water-soluble aerosol fraction in Mexico City, *J. Geophys. Res.*, *115*, D09204, doi:10.1029/2009JD013195.

1. Introduction

[2] It is well known that the ability of aerosols to act as cloud condensation nuclei (CCN) is a strong function of their size, chemical composition, and supersaturation levels in ambient clouds. The compositional complexity of aerosol, especially for the organic fraction, poses a challenge for its description in atmospheric models of aerosol-cloud interactions. Knowledge of their cumulative impact on CCN activity is nevertheless important, as carbonaceous material can constitute up to 90% of the total aerosol [e.g., *Andreae and Crutzen*, 1997; *Moffet et al.*, 2008; *Stone et al.*, 2008], 10–70% of which is water-soluble [*Facchini et al.*, 2000; *Hagler et al.*, 2007; *Sullivan et al.*, 2004; *Zappoli et al.*, 1999].

[3] Many studies have focused on understanding the effects of water-soluble organic compounds on CCN activity [e.g., *Asa-Awuku et al.*, 2008; *Dinar et al.*, 2006b; *Svenningsson et al.*, 2006], hygroscopicity [e.g., *Badger et al.*, 2006; *Brooks et al.*, 2004; *Dinar et al.*, 2007; *Svenningsson et al.*, 2006; *Wex et al.*, 2007], droplet activation kinetics [e.g., *Asa-Awuku et al.*, 2009; *Engelhart et al.*, 2008; *Ruehl et al.*, 2008, 2009], and surface tension [e.g., *Asa-Awuku et al.*, 2008; *Kiss et al.*, 2005; *Taraniuk et al.*, 2007]. Chemical

[1]School of Chemical and Biomolecular Engineering, Georgia Institute of Technology, Atlanta, Georgia, USA.
[2]School of Earth and Atmospheric Sciences, Georgia Institute of Technology, Atlanta, Georgia, USA.
[3]Now at Center for Atmospheric Particle Studies, Carnegie Mellon University, Pittsburgh, Pennsylvania, USA.
[4]School of Civil and Environmental Engineering, Georgia Institute of Technology, Atlanta, Georgia, USA.
[5]Now at Department of Atmospheric Science, Colorado State University, Fort Collins, Colorado, USA.

0148-0227/10/2009JD013195

characterization of the organics in ambient samples using analytical techniques such as size exclusion chromatography and mass spectrometry [*Kiss et al.*, 2003; *Samburova et al.*, 2005; *Zappoli et al.*, 1999] cannot identify the majority of compounds present. Even if complete speciation were possible, the amount of information produced is challenging to implement in models of aerosol-cloud interactions. Alternatively, indirect methods can be used to infer and parameterize the CCN properties of the organic fraction. *Petters and Kreidenweis* [2007] proposed the use of a hygroscopicity parameter, κ (a parameterized Raoult term in Köhler theory), which is being widely adopted to express the aerosol water uptake characteristics and CCN activity of aerosol with a wide range of compositions. *Wex et al.* [2007] suggested another single parameter approach, the ionic density, ρ_{ion}, to model the hygroscopic growth of Humic-Like Substances (HULIS). Köhler Theory Analysis (KTA) [*Padró et al.*, 2007; *Asa-Awuku et al.*, 2008, 2010; *Moore et al.*, 2008; *Engelhart et al.*, 2008] uses measurements of size-resolved CCN activity and surface tension to infer the molar volume of organics. In the absence of surface tension measurements, a form of KTA can be applied to deconvolute the contribution of solute and surface tension depression to the observed CCN activity [*Moore et al.*, 2008; *Asa-Awuku et al.*, 2009]. KTA is most successfully applied when the organic fraction in the aerosol is large and the inorganic ion concentration and amount of water-soluble organic carbon (WSOC) is known [*Padró et al.*, 2007].

[4] Studies to date using ambient data to constrain κ for organic aerosol often focus on the value of the parameter, and less on the origin of the hygroscopicity (e.g., soluble fraction, molar volume, and surface tension depression). The latter is important, as κ, when predicted in models, is calculated as the volume-fraction weighted average of the hygroscopicity of each aerosol constituent. Surface tension effects do not obey "volume additivity," so estimations of κ assuming a constant surface tension could be biased. For example, *Engelhart et al.* [2008] found that κ ranged between 0.11 and 0.14 for secondary organic aerosol (SOA) originating from monoterpene SOA. However, KTA of the water-soluble fraction of the SOA suggests that ~60% of the aerosol is soluble, implying that the true hygroscopicity parameter for the monoterpene SOA is 40% lower (i.e., κ = 0.06–0.084). The unaccounted ~10% surface tension reduction (with respect to pure water) leads to the 40% overestimation of organic hygroscopicity. Surface tension reduction can still be present even if the SOA is mixed with large amounts of electrolytes, so that the aerosol would exhibit a higher hygroscopicity than expected from simple volume additivity of κ.

[5] In this study we characterize the CCN relevant properties (i.e., hygroscopicity parameter, surface tension, molar volume, and droplet activation kinetics) of the water-soluble fraction of Mexico City (MC) aerosol collected during March 2006. Emphasis is placed on constraining the impact of water-soluble organics on droplet formation (observing the activation kinetics and deconvoluting surface tension from solute contributions to the hygroscopicity) and their temporal variation. Mexico City was selected for sample collection as it represents an environment with strong anthropogenic influences (e.g., biomass burning, fossil fuel, and dust). Collection at two sites allows comparison of aged/background properties against fresh emissions at downtown Mexico City.

2. Location Description, Sample Collection, and Experimental Methods

2.1. Location, Meteorology, and Air Masses Sampled

[6] The main goal of MILAGRO (Megacity Initiative: Local and Global Research Observations; http://www.eol.ucar.edu/projects/milagro/) was to study the evolution of the Mexico City plume as it aged and quantify its impact on local and regional scales. Mexico City was chosen owing to its size, pollution level, meteorology, and geography. The field campaign took place in March, which is characterized by dry, clear sky conditions with strong photochemistry [*Jáuregui Ostos*, 2000] and a low frequency of biomass burning events. By selecting this period, the evolution of the Mexico City plume could be studied without interference from regional biomass burning events [*Fast et al.*, 2007]. Airborne and ground-based measurements were performed at three sites: (1) the "T0" site, at Instituto Mexicano de Petróleo (19.488°N, 99.147°W; Mexico City), (2) the "T1" site, at the Universidad Tecnológica de Tecámac (19.703°N, 98.982°W; Tecámac, Estado de México, Northeast of the city), and (3) the "T2" site, at Pachuca (20.010°N, 98.909°W). The design of the campaign and site selection was based on prevailing meteorology and the MCMA-2003 campaign results [*Molina et al.*, 2007]. The T0 site was chosen in the metropolitan area to represent fresh emissions while the T1 and T2 sites were chosen outside of the city limits to study the effects of transport mixing and chemical aging on plume properties. Filter samples considered in this study were collected at the T0 and T1 sites.

[7] Three periods characterized the overall meteorological conditions throughout MILAGRO [*Fast et al.*, 2007]. The first period was prior to 14 March, where clear sky and dry conditions (relative humidity, RH < 50%) persisted. The second period (14–23 March) was characterized by a sharp increase in RH (55–85%) and the development of late afternoon convection associated with the passage of a weak cold front on 14 March. The last and third period (after 23 March) began with the passage of a strong cold front which led to an increase in RH, afternoon convection, and stronger precipitation events than those observed during the second period. As a result, the frequency and intensity of fires within the vicinity of Mexico City during this period diminished [*Fast et al.*, 2007]. Therefore, interaction between Mexico City and biomass burning plumes occurred mostly during the first 3 weeks of MILAGRO.

[8] Tracer simulations using the WRF-Chem model suggest that the most direct transport between the T0 and T1 sites occurred from 9–10 March and 18–20 March [*Fast et al.*, 2007]. Further analysis of measurements and large-scale analysis of the winds suggested favorable days of transport from T0 to T1 to have occurred during 8–12 March and 17–30 March [*Fast et al.*, 2007].

2.2. Particle Collection and Extraction

[9] Ambient aerosols of aerodynamic diameter less than 2.5 μm ($PM_{2.5}$) were collected on quartz filters with Thermo Andersen Hi-Volume samplers. Three Hi-Volume samplers

Table 1. Summary of Filter Grouping With Extracted WSOC Concentration, Inferred Average Organic Molecular Weight, and Hygroscopicity Parameter[a]

Sample Name (Sample Period)	Collection Date (March)	C_{WSOC} (ppm)	M_{org} (g mol^{-1})	In Situ κ[b]	κ_{CCN}[c]
MEX-T0-1 (24 h)	18–19	287.5 ± 1.44	N/A[d]	N/A[e]	0.319 ± 0.055
MEX-T0-2 (24 h)	20–21	310 ± 0	N/A[d]	N/A[e]	0.288 ± 0.073
MEX-T0-3 (12 h day)	22–24	246.25 ± 0.43	N/A[d]	N/A[e]	0.271 ± 0.046
MEX-T0-4 (12 h day)	25–27	715 ± 5.2	N/A[d]	N/A[e]	0.252 ± 0.019
MEX-T0-5 (12 h day)	28–30	237.75 ± 3.08	N/A[d]	N/A[e]	0.290 ± 0.107
MEX-T1-1 (24 h)	9, 11	392.5 ± 1.44	158.31 ± 56.41	N/A[e]	0.339 ± 0.094
MEX-T1-2 (24 h)	13, 16	317.5 ± 1.44	141.81 ± 11.73	~0.25	0.316 ± 0.052
MEX-T1-3 (24 h)	17–18	115.5 ± 0.95	161.92 ± 11.79	~0.30	0.329 ± 0.024
MEX-T1-4 (24 h)	15–16	217 ± 0.63	222.71 ± 15.67	~0.25	0.297 ± 0.029
MEX-T1-5 (24 h)	17–18	110.5 ± 0.80	N/A[d]	0.25–0.30	0.311 ± 0.025
MEX-T1-6 (24 h)	19	117.5 ± 2.5	61.93 ± 6.18	~0.30	0.366 ± 0.017
MEX-T1-7 (12 h night)	20–22	114.5 ± 0.72	N/A[d]	~0.20	0.220 ± 0.017
MEX-T1-8 (12 h night)	23–25	76.75 ± 3.48	431.35 ± 210.28	~0.20	0.221 ± 0.023
MEX-T1-9 (12 h night)	26–28	140.75 ± 1.42	344.64 ± 117.61	N/A[e]	0.275 ± 0.030
MEX-T1-10 (12 h day)	21–23	382.5 ± 1.44	380.82 ± 97.00	0.20–0.25	0.214 ± 0.013
MEX-T1-11 (12 h day)	24–26	352.5 ± 1.44	221.97 ± 8.08	~0.25	0.263 ± 0.010
MEX-T1-12 (12 h day)	27–29	362.5 ± 1.44	267.89 ± 13.94	N/A[e]	0.256 ± 0.006

[a]Also shown is κ derived from concurrent in situ aerosol measurements [*Lance*, 2007]. C_{WSOC}, WSOC concentration; M_{org}, inferred average organic molecular weight; and κ, hygroscopicity parameter.
[b]Obtained from in situ CCN activity measurements of 100 nm aerosol at T1 [*Lance*, 2007].
[c]Calculated by application of equation (6), assuming the surface tension of water.
[d]Organic mass fraction insufficiently high for application of KTA.
[e]CCN measurements not available at location or time.

were used for aerosol collection: one located at T0 (on the rooftop of a building approximately 20 m above ground level), and two located at ground level at the T1 site. Twenty-four and 12 h integrated samples at T0 were collected from 18 to 21 March and from 22 to 30 March, respectively. At T1, 24 h samples were obtained from 9 to 19 March, and 12 h samples from 20 to 30 March. At T1, 12 h integrated samples were collected during daytime (0600 to 1800, Local Standard Time (LST)) and nighttime (1800 to 0600 LST); only daytime samples were collected at T0. Aerosol collection for the 24 h samples started at 1000 LST at both locations.

[10] The Hi-Volume samplers draw 1.16 m^3 min^{-1} of air over a two stage impactor assembly to separately collect particles from 10 to 2.5 μm and below 2.5 μm diameter. The quartz filters used in our study were pretreated to remove organic residue and excess water vapor by baking them using the procedure of *Sullivan and Weber* [2006]. After particle collection in the field, the filters were stored in a freezer to limit losses of volatile components until the WSOC is analyzed in the laboratory. Processing of the filter samples involve extraction of the WSOC fraction in water. Since a high-concentration sample is needed to perform the surface tension measurements, multiple filters are extracted at a time resulting in a sample with ~400 ppm of WSOC. Filters were grouped by integration periods (Table 1) and placed in a Nalgene HDPE bottle with 125 mL of dionized (DI) water for extraction. Two 24 h filters were placed in each bottle, and three for 12 h filters. Each bottle was placed on a sonicator and heated in a water bath (with temperature ~60°C) [*Baumann et al.*, 2003; *Sullivan and Weber*, 2006] for 75 min. The solution was then allowed to cool down for 3 h and filtered through a 0.45 μm pore syringe filter to remove quartz fibers and insoluble particles suspended in solution. The organic carbon concentration (C_{WSOC}) in all of the extracts was measured with a Total Organic Carbon (TOC) analyzer (section 2.3.1). The heating accelerates the dissolution of the particles collected in the filter, while the cooling step allows the repartitioning of semivolatile species back into solution. It is possible that some carbon loss and chemical alterations of the sample may have occurred. Application of this technique however to aerosol collected from chamber SOA experiments [*Engelhart et al.*, 2008; *Asa-Awuku et al.*, 2009] provided properties for the WSOC that is consistent with known speciation. This suggests that water extraction may not substantially alter the properties of the WSOC.

[11] The Hi-Volume samplers used are not denuded making them susceptible to positive artifacts from the absorption of organic vapors on the collected aerosols and quartz filter fibers [*Turpin et al.*, 1994; *Sullivan and Weber*, 2006]. The extent of these artifacts were assessed by *Sullivan and Weber* [2006], by comparing WSOC from online (PILS-WSOC) and offline (filters) measurements similar to those presented in were performed. WSOC concentrations from filter extracts were found to be about 20% higher than the online measurements; therefore we are addressing an upper bound in amount of water-soluble organics present in the aerosol.

[12] Although grouping the filters allowed us to have enough mass for CCN measurements, the extract was not concentrated enough for surface tension measurements representative of CCN at the point of activation (1000–10,000 ppm). This is addressed by concentrating the samples using a rotary evaporator (rotavap; Büchi R-124), which removes water with flash evaporization under vacuum at ~75°C. The water evaporated from the sample is recondensed, while the concentrated WSOC solution remains in the evaporation flask. A carbon balance calculation shows that most of the WSOC (84–98%) remains in the concentrated sample.

2.3. Chemical Composition Measurements

2.3.1. TOC Analyzer

[13] WSOC concentration for all samples was measured with a portable TOC analyzer (Sievers 900). Organic carbon concentration is quantified in the sample by subtracting the inorganic carbon concentration from the total carbon present. Inorganic and total carbon concentration is determined by measuring the amount of carbon dioxide formed during the acidification (for inorganic carbon) and oxidation (for total carbon) of the sample streams. Prior to each measurement, samples were diluted by a factor of 250 or 1000 to ensure the WSOC concentration lies within the dynamic range of the instrument (0.20 ppb to 10 ppm). Measurement of WSOC was repeated three times for each sample.

2.3.2. Ion Chromatography

[14] Ion chromatography (IC) was used to measure the concentration of the major ions in solution. The IC used in this study (Dionex Model DX500) has two channels, allowing for the measurement of anions and cations. An assessment of the instrument is given by *Butler* [2000] and *Cobb* [2006]. Anions measured included acetate ($C_2H_3O_2^-$), chloride (Cl^-), formate ($HCOO^-$), nitrate (NO_3^-), nitrite (NO_2^-), oxalate ($C_2O_4^{2-}$), and sulfate (SO_4^{2-}). The cations measured were ammonium (NH_4^+), calcium (Ca^{2+}), potassium (K^+), and sodium (Na^+). The samples were diluted by a factor of 50 to be within the dynamic range of the standards used for the IC calibration. The ion concentrations obtained from the IC measurement were then used as input for the ISORROPIA-II thermodynamic equilibrium code [*Fountoukis and Nenes*, 2007] (http://nenes.eas.gatech.edu/ISORROPIA) to predict the mixture of inorganic salts dissolved in the samples (used in the application of KTA and κ-Köhler theory discussed in section 3).

2.4. Surface Tension

[15] The surface tension of each sample was measured with a pendant drop tensiometer (CAM 200 Optical Contact Angle Meter, by KSV Inc.). A mechanically controlled microsyringe was used to produce a droplet of sample at the tip of a stainless steel needle. A picture of the drop is then taken at the point where the drop is ready to fall from the tip. The sample surface tension, σ, is then determined by fitting the droplet shape to the Young-Laplace equation [*Spelt and Li*, 1996]. Approximately 10 pictures per droplet were taken to obtain an average and standard deviation for surface tension.

[16] Surface tension depression depends on the surfactant concentration (expressed by C_{WSOC}, the concentration of dissolved carbon), and is measured for each extract concentration on the rotavap, and at 3:1, 2:1, 1:1, 1:3, and 1:∞ dilutions with ultrafine pure water (Fisher). The σ is then expressed against C_{WSOC} (ppm C; 1 ppm = 1 mg L^{-1} for a solution of unit density) for each sample and fit to the Szyskowski-Langmuir equation [*Langmuir*, 1917],

$$\sigma = \sigma_w - \alpha T \ln(1 + \beta C_{WSOC}), \quad (1)$$

where σ_{w} is the surface tension of water at temperature T of measurement, and the parameters α and β are obtained by least squares minimization of equation (1) to the data.

2.5. Measurements of CCN Activity and Droplet Activation Kinetics

[17] The laboratory setup employed to characterize the CCN activity of the dissolved material and the impact of organic material on the droplet activation kinetics is described by *Padró et al.* [2007] and *Asa-Awuku et al.* [2008]. The system consists of an aerosol generation, size classification, and CCN measurement section. Polydisperse aerosols are generated by atomizing the filter extracts. The droplets are subsequently dried by flowing them through multiple diffusion driers and charged with a Kr-85 bipolar charger (TSI Model 3077). A Differential Mobility Analyzer (DMA, TSI Model 3081L) is then used for size mobility selection of the dry particles. The classified aerosol flow is split into two streams, one sent to a Condensation Particle Counter (CPC, TSI Model 3022A) to measure their concentration (CN) and the other to a Continuous Flow Streamwise Thermal Gradient CCN Chamber (CFSTGC) [*Lance et al.*, 2006; *Roberts and Nenes*, 2005] to measure the fraction that act as CCN. The activated droplets in the CCN are counted and sized at the exit with an Optical Particle Counter (OPC, 660 nm) with a dynamic range of 0.75 to 10 μm with 0.5 μm bin resolution.

[18] In this work, CCN activation data is obtained using Scanning Mobility CCN Analysis (SMCA) [*Asa-Awuku et al.*, 2009; *Moore et al.*, 2008; R. Moore et al., Scanning Mobility CCN Analysis—A method for fast measurements of size resolved CCN distributions and activation kinetics, submitted to *Aerosol Science and Technology*, 2010]; instead of "stepping" through the DMA voltage to obtain CCN concentrations at discrete values of mobility diameter, the DMA voltage is continuously changed over time, so that the dynamic mobility range of the DMA is "scanned" over 2 min. During a size scan, the supersaturation in the CFSTGC is maintained constant. The time series of activated droplet size, CCN, and CN counts are then inverted to obtain size-resolved CCN activity and activation kinetics. In this study, the aerosol size was ranged between 7 and 260 nm, and 0.2% to 1.2% supersaturation.

[19] CCN activity of the aerosol is characterized by determining the minimum dry diameter, d_{p50}, of particles that activate into cloud droplets at each supersaturation (i.e., those particles with a critical supersaturation equal to the instrument supersaturation). The d_{p50} is found by expressing the ratio of CCN to CN concentration with respect to dry particle diameter and determining the dry diameter for which 50% of the aerosol act as CCN. To facilitate the analysis, the activation data is fit to a sigmoid curve which neglects the impact of multiply charged particles; d_{p50} then corresponds to the inflection point of the sigmoid. Once the d_{p50} at each supersaturation is known, a "CCN spectrum" (s_c versus d_{p50}) can be obtained and used to characterize the average properties of WSOC using Köhler Theory Analysis or κ-Köhler Theory (section 3).

[20] The CCN instrument used in this study was calibrated with $(NH_4)_2SO_4$ using a procedure similar to that of *Sorooshian et al.* [2008], *Asa-Awuku et al.* [2009], and *Rose et al.* [2008]. The calibration procedure consisted of generating particles by atomizing a $(NH_4)_2SO_4$ solution. The polydisperse aerosol was then dried, charged, and size selected with a DMA operated in scanning voltage mode

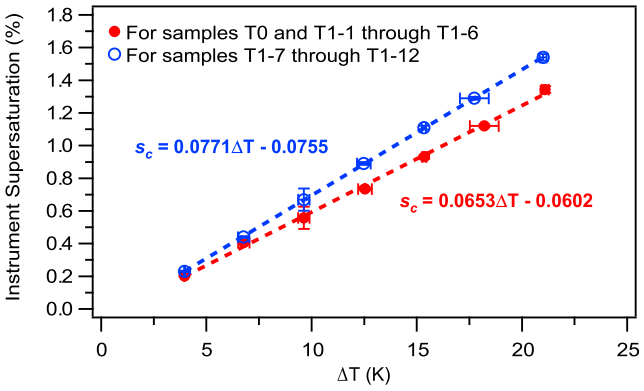

Figure 1. Instrument supersaturation versus delta T. Calibration was performed at a flow rate of 500 cm^3 min^{-1} and at ambient pressure using $(NH_4)_2SO_4$ aerosol.

(SMCA). The effective supersaturation in the column was determined from d_{p50} using traditional Köhler theory, with osmotic coefficients calculated with the Pitzer activity coefficient model [*Clegg and Brimblecombe*, 1988; *Pitzer and Mayorga*, 1973] and the surface tension of water (calculated at the average column temperature). The uncertainty in supersaturation was determined from Köhler theory and the standard deviation observed in the d_{p50}. This procedure is repeated for multiple values of ΔT, for which calibration curves of instrument supersaturation versus ΔT are generated. The resulting calibration curves are shown in Figure 1.

[21] CCN activation kinetics and changes thereof from the presence of organics can also be determined from the CCN measurements. This is done by monitoring the droplet size measured at the OPC for particles of critical supersaturation equal to the instrument supersaturation (i.e., dry diameter equal to d_{p50}). For particles composed of pure deliquescent electrolytes (e.g., $(NH_4)_2SO_4$ calibration aerosol), CCN activation kinetics is rapid (corresponding to an uptake coefficient of ~0.1) and the wet droplet size, D_w, corresponding to the d_{p50} particles is used as a reference (for the given conditions of pressure, ΔT, and flow). Comparing D_w against the corresponding wet diameter (i.e., same critical supersaturation) of activated particles generated from the extracted filters can reveal whether organic compounds retard activation kinetics. This technique, called "Threshold Droplet Growth Analysis (TDGA)," has been successfully applied to a number of in situ [*Sorooshian et al.*, 2008; *Bougiatioti et al.*, 2009; *Murphy et al.*, 2009; *Lance et al.*, 2009] and laboratory [*Moore et al.*, 2008; *Engelhart et al.*, 2008; *Asa-Awuku et al.*, 2009, 2010] studies. When combined with a computational fluid dynamics model of the CCN instrument [*Lance et al.*, 2006], changes in droplet size can then be parameterized in terms of changes in the water vapor uptake coefficient [*Asa-Awuku et al.*, 2009; *Engelhart et al.*, 2008; *Ruehl et al.*, 2008, 2009].

2.6. Effects of Electrolyte Addition on Surface Tension and CCN Activity

[22] The presence of inorganic solute at high concentrations may enhance the presence of organics at the droplet-air interface and affect surface tension [*Asa-Awuku et al.*, 2008; *Kiss et al.*, 2005]. To explore this potential, prescribed amounts of $(NH_4)_2SO_4$, m_{AS}, as multiples of the existing organic mass, is added to the sample:

$$m_{AS} = f m_{org} \tag{2}$$

where f is the "mass addition factor," m_{org} is the mass of dissolved organic matter in the sample (mg), given by, $m_{org} = [\frac{OM}{OC}]C_{WSOC}V_{sample}$, V_{sample} is the sample volume (L), and OM/OC is the organic matter-to-organic carbon ratio, assumed to be 1.5 for T0 and 2.3 for T1 [*DeCarlo et al.*, 2008; *Aiken et al.*, 2008]. Different OM/OC values are used at each site to reflect the oxidation state of the aerosol at each location. Lower OM/OC ratios correspond to fresher emissions (T0) while larger values to aged regional air (T1).

3. Experimental Analysis

3.1. Köhler Theory Analysis

[23] Köhler Theory Analysis is used to infer average thermodynamic properties (e.g., molar volume) of the water-soluble organic fraction of the aerosol. The method is based on combining Köhler theory with size-resolved CCN, chemical composition, and surface tension measurements [*Padró et al.*, 2007]. When combined with SMCA (R. Moore et al., submitted manuscript, 2010), KTA allows the characterization of the CCN relevant properties of ambient WSOC from small amount of sample typically collected on filters. KTA has been evaluated for laboratory generated particles composed of inorganic-organic mixtures of known composition [*Padró et al.*, 2007], biomass burning WSOC [*Asa-Awuku et al.*, 2008], secondary organic aerosol [*Asa-Awuku et al.*, 2009, 2010; *Engelhart et al.*, 2008], and primary marine organic matter [*Moore et al.*, 2008].

[24] According to KTA, the average molar volume, $\frac{M_{org}}{\rho_{org}}$, of the soluble organic fraction of an aerosol is given by

$$\frac{M_{org}}{\rho_{org}} = \frac{\varepsilon_{org}\upsilon_{org}}{\frac{256}{27}\left(\frac{M_w}{\rho_w}\right)^2\left(\frac{1}{RT}\right)^3\sigma^3\omega^{-2} - \sum_{inorg}\left(\frac{\rho}{M}\right)_{inorg}\varepsilon_{inorg}\upsilon_{inorg}}, \tag{3}$$

where M_{org}, ε_{org}, υ_{org}, ρ_{org}, is the molar mass, dry volume fraction, effective van't Hoff factor, and density of the organic fraction, respectively; and M_{inorg}, ρ_{inorg}, ε_{inorg}, and υ_{inorg} are the molecular mass, density, dry volume fraction, and effective van't Hoff factor of the inorganic compounds present in the aerosol sample (Table 2), respectively. M_w and ρ_w are the molar mass and density of water, respectively, R is the ideal gas constant, T is the temperature, and σ is the surface tension of the solution at the point of activation. The Pitzer activity coefficient model [*Clegg and Brimblecombe*, 1988; *Pitzer and Mayorga*, 1973] is used to calculate the effective υ_{inorg} for all inorganic salts present in the samples, at the concentration corresponding to the critical wet diameter of the CCN [*Padró et al.*, 2007]. The ω is the "Fitted CCN Activity" (FCA) parameter [*Padró et al.*, 2007], obtained by expressing CCN activity measurements by the

Table 2. Properties of Inorganic Salts Potentially Present in the Extracted Filters

Compound Name	Chemical Formula	Molar Mass (g mol^{-1})	ρ[a] (g cm^{-3})	κ
Ammonium bisulfate	NH_4HSO_4	115.11	1.79	0.53
Ammonium chloride	NH_4Cl	53.49	2.165	1.46
Ammonium nitrate	NH_4NO_3	80.04	1.5	0.64
Ammonium sulfate	$(NH_4)_2SO_4$	132.14	1.77[b]	0.60
Calcium carbonate	$CaCO_3$	100.09	2.71	<0.01
Calcium chloride	$CaCl_2$	110.98	2.15	0.70
Calcium nitrate	$Ca(NO_3)_2$	164	1.82	0.40
Calcium sulfate	$CaSO_4$	136.14	2.32	<0.01
Letovicite	$(NH_4)_3H(SO_4)_2$	247.25	1.83	0.60
Potassium bisulfate	$KHSO_4$	136.17	2.24	0.59
Potassium sulfate	K_2SO_4	174.27	2.66	0.69
Sodium bisulfate	$NaHSO_4$	120.06	2.742	0.82
Sodium sulfate	Na_2SO_4	142.04	2.68	0.85
Sulfuric acid	H_2SO_4	98.08	1.84	0.81

[a]Unless noted, values are from the Material Safety Data Sheet.
[b]*Svenningsson et al.* [2006].

power law expression $s_c = \omega d_{50}^{-3/2}$. The volume fraction of substance "*i*," ε_i, is computed as follows:

$$\varepsilon_i = \frac{x_i/\rho_i}{\sum_j (x/\rho)_j}, \quad (4)$$

where x_i is the mass fraction of the compound of interest, and *j* refers to all compounds present in the aerosol (organic or inorganic; Tables 3 and 4). The ionic composition of each sample (obtained from the IC) is converted into a mixture of salts by applying the ISORROPIA-II model as described in section 2.3.2. OM is assumed to have density of 1.6 g cm^{-3} [*Dinar et al.*, 2006a] at T0 and a density of 1.5 g cm^{-3} at T1 [*Cross et al.*, 2009].

[25] The uncertainty in the inferred organic molar mass, ΔM_{org}, can be estimated from the total uncertainty from each parameter as

$$\Delta M_{org} = \sqrt{\Sigma(\Phi_z \Delta z)^2}, \quad (5)$$

where Φ_z is the sensitivity of the organic molar mass to a parameter, *z*, that affects M_{org} (i.e., σ, ω, υ_{org}, υ_{inorg}, ε_{org}, and ε_{inorg},), $\Phi_z = \frac{\partial M_{org}}{\partial z}$, and Δz is the uncertainty on *z*. The formulas used to compute the sensitivity of the organic molar mass to *z* are shown in Table 5.

3.2. The κ-Köhler Theory Analysis

[26] The κ-Köhler theory was introduced by *Petters and Kreidenweis* [2007] to represent aerosol hygroscopic water uptake and CCN activity through the "hygroscopicity parameter," κ, that collectively accounts for density, molar mass, and dissociation effects of solute on water activity (the "Raoult term" in the Köhler equation). The κ values range from 0.0 to 2, with hygroscopic inorganic species such as $(NH_4)_2SO_4$ and NaCl having κ ranging from 0.5 to 2 and organic species and mixtures ranging from 0.01 to 0.5. For $\kappa > 0.01$, "simple" Köhler theory applies and the hygroscopicity parameter can be obtained from s_c and d_{p50} pairs as

$$\kappa = \frac{4A^3}{27 d_{p50}^3 s_c^2}, \quad (6)$$

where $A = \frac{4M_w\sigma_w}{RT\rho_w}$ and s_c is the instrument supersaturation. The κ is calculated using the surface tension of water evaluated at the median column temperature [*Petters and Kreidenweis*, 2007].

[27] Surface tension of the CCN can be different from water if surfactants (e.g., HULIS) are present [*Dinar et al.*, 2007; *Kiss et al.*, 2005]. This can introduce notable uncertainty in κ calculations, the extent of which can be evaluated from equation (6). If the surface tension depression from pure water at the point of activation is $\Delta\sigma$, then the true value of κ is a factor of $(1 - \frac{\Delta\sigma}{\sigma_w})^{-3}$ lower. For example, for a 10% depression ($\Delta\sigma/\sigma_w = 0.10$), κ is ~30% lower than the values inferred when the surface tension of pure water is assumed.

4. Results and Discussion

4.1. Surfactant Characteristics

[28] Table 6 presents the fitted Szyskowski-Langmuir adsorption constants α and β (equation (1)), the maximum C_{WSOC} of the extracted and concentrated sample, and the concentration of SO_4^{2-} ions in solution (C_{SO4}). The surface tension depression is also presented at $C_{\mathrm{WSOC}} = 1000$ ppm for comparison purposes. Even though organics at both locations depress σ, stronger depression is seen at T0 (24 h samples, Figure 2a; 12 h day samples, Figure 2b) consistent with having a higher hydrophobic fraction (lower O/C ratio) very near emission sources [*DeCarlo et al.*, 2008; *Kleinman et al.*, 2008]. The observed surface tension depression at the T0 site (for both sample periods) could further be enhanced by the higher salt concentration present at this site, as suggested by the enhanced surface tension depression seen in the salted samples (Table 6).

[29] Differences were observed in surfactant characteristics between the day and night samples at T1, with nighttime samples being slightly more surface active than the day samples (Figure 2c). Higher σ depression observed in the nighttime samples may reflect influence from primary emissions (which tend to be more hydrophobic than SOA

Table 3. Organic and Inorganic Mass Fraction and Inorganic Fraction Hygroscopicity Parameter for Mexico City T0 Site Samples[a]

Sample	x_{org}	$x_{Na_2SO_4}$	x_{NaHSO_4}	$x_{(NH_4)_2SO_4}$	$x_{NH_4HSO_4}$	$x_{(NH_4)_3H(SO_4)_2}$	x_{CaSO_4}	$x_{K_2SO_4}$	x_{KHSO_4}	$x_{H_2SO_4}$	κ_{inorg}
MEX-T0-1	0.22	0	0.21	0	0.29	0	0.11	0	0.02	0.16	0.593
MEX-T0-2	0.27	0	0.19	0	0.30	0	0.10	0	0.02	0.12	0.576
MEX-T0-3	0.25	0.07	0.13	0	0.41	0	0.11	0.03	0	0	0.525
MEX-T0-4	0.55	0.11	0	0.13	0	0.12	0.08	0.02	0	0	0.555
MEX-T0-5	0.35	0.17	0	0.36	0	0	0.10	0.02	0	0	0.573

[a]Salts shown for each sample were predicted by using ISORROPIA II [*Fountoukis and Nenes*, 2007]. Uncertainties in all mass fractions are less than 0.3%.

Table 4. Organic and Inorganic Mass Fraction and Organic and Inorganic Fraction Hygroscopicity Parameters for Mexico City T1 Site Samples[a]

Sample	x_{org}	$x_{(NH_4)_2SO_4}$	$x_{NH_4NO_3}$	x_{NH_4Cl}	x_{CaSO_4}	$x_{Ca_2(NO_3)_2}$	x_{CaCl_2}	$x_{Na_2CO_3}$	x_{CaCO_3}	$x_{K_2CO_3}$	$x_{Na_2SO_4}$	$x_{K_2SO_4}$	κ_{inorg}	κ_{org}
MEX-T1-1	0.72	0.08	0	0	0.10	0	0	0.02	0	0	0.06	0.03	0.415	0.171
MEX-T1-2	0.67	0.12	0	0	0.06	0	0	0.06	0.08	0.02	0	0	0.264	0.190
MEX-T1-3	0.49	0.17	0	0	0.02	0	0	0.07	0.21	0.04	0	0	0.255	0.167
MEX-T1-4	0.57	0.12	0.03	0.02	0	0	0	0.07	0.16	0.03	0	0	0.331	0.121
MEX-T1-5	0.39	0.21	0.01	0	0	0.06	0	0.12	0.17	0.04	0	0	0.314	N/A[b]
MEX-T1-6	0.44	0.12	0	0	0.14	0	0	0.17	0.09	0.06	0	0	0.157	0.436
MEX-T1-7	0.50	0.14	0.05	0	0	0.01	0	0.16	0.11	0.03	0	0	0.305	N/A[b]
MEX-T1-8	0.52	0.09	0.02	0	0	0.02	0	0.20	0.11	0.02	0	0	0.212	0.063
MEX-T1-9	0.58	0.09	0.06	0.01	0	0	0.03	0.17	0.04	0.02	0	0	0.352	0.078
MEX-T1-10	0.70	0.09	0.02	0	0	0.01	0	0.10	0.07	0.02	0	0	0.290	0.071
MEX-T1-11	0.68	0.06	0.04	0.01	0	0	0.003	0.14	0.07	0.01	0	0	0.282	0.122
MEX-T1-12	0.74	0.06	0.05	0	0	0	0.01	0.09	0.04	0.01	0	0	0.360	0.101

[a]Salts shown for each sample were predicted by using ISORROPIA II [*Fountoukis and Nenes*, 2007]. Uncertainties in all mass fractions are smaller than 0.3%.
[b]Organic mass fraction insufficiently high for application of KTA.

produced during the daytime), or, aging of hygroscopic SOA (formed during daytime photochemical production) in the aqueous phase to form HULIS [*Hoffer et al.*, 2004]. A source apportionment study performed for the fine organic aerosol for T0 and T1 sites found particulates at T1 to be influenced by local sources rather than from the Mexico City outflow [*Stone et al.*, 2008].

4.2. CCN Activity and Hygroscopicity

[30] The CCN activity (embodied in the s_c versus d_{p50} relationship) of aerosol generated from some of the extracted samples is presented in Figure 3. The curves shown are grouped by sites and integration period (Figures 3a and 3b) as well as the time of day for the T1 samples (Figure 3c). As a first approximation, the extracts were found to have similar CCN activity regardless of the site (Figures 3a and 3b). Compared to T1 samples, T0 samples tend to have somewhat higher CCN activity (i.e., the s_c-d_{p50} curve is closer to that of $(NH_4)_2SO_4$) due to the stronger surface tension depression and the higher salt fraction in the latter samples (Tables 3 and 4). The CCN activity of 12 h (day and night) samples collected at T1 (Figure 3c) presents little variability.

[31] The κ was calculated from application of equation (6) to the s_c and d_{p50} pairs (Table 1). For the T0 site samples, κ ranged between 0.29–0.32 (24 h filters) and 0.25–0.39 (12 h filters). The κ for the T1 site samples ranged from 0.30 to 0.37 (24 h filters), 0.21 to 0.26 (12 h day filters), and 0.22 to 0.28 (12 h night filters). The overall average is 0.28 ± 0.06. These values of κ are consistent with soluble salts and very hygroscopic organics [*Carrico et al.*, 2008; *Koehler et al.*, 2009; *Petters and Kreidenweis*, 2007; *Shantz et al.*, 2008]. The κ values obtained at the T1 site are also consistent with those derived from concurrent in situ CCN measurements [*Lance*, 2007] (Table 1), indicating that the material obtained from the filter water extraction reflects the hygroscopic properties of the ambient aerosol. Given that the aerosol from filter extracts is completely soluble, one expected that its κ will be higher than the in situ (parent) aerosol. Indeed this is the case [*Lance*, 2007] (Table 1). No significant correlation was found between κ and the organic mass fraction or sampling site (Figure 4; $R^2 = 0.01$).

[32] The invariance of κ with respect to soluble organic fraction although counterintuitive, provides insight on the nature of the WSOC. First, the water-soluble components extracted from both sites have about the same hygroscopicity, suggesting that aging processes may not affect its overall hygroscopicity (although their detailed speciation may vary considerably) but only their relative amount in the aerosol. Second, the hygroscopicity of the water-soluble organic (i.e., κ for $x_{org} \rightarrow 1$) and inorganic fractions (i.e., κ for $x_{org} \rightarrow 0$) are very similar (Figure 4); this invariance may reflect a compensation between solute (when $x_{org} \rightarrow 0$) and surface tension depression (when $x_{org} \rightarrow 1$) effects. Also, $\kappa \rightarrow 0.4$ for $x_{org} \rightarrow 0$ (Figure 4), which is somewhat lower than values for mixtures of electrolytes (~0.6 and above). This is likely because the inorganic fraction is predicted to contain a fair amount of $CaSO_4$ and $CaCO_3$ that dissolves completely during the water extraction process, but to a much lesser degree in the limited amounts of water in CCN at their critical wet diameter (Tables 2, 3, and 4).

Table 5. Formulas Used for Computing the Sensitivity of Organic Molar Mass to σ, ω, υ_{org}, υ_{inorg}, ε_{org}, and ε_{inorg}

Parameter, z	Sensitivity, $\Phi_z = \frac{\partial M_{org}}{\partial z}$
σ	$\Phi_\sigma = \frac{768}{27}\left(\frac{M_w}{\rho_w}\right)^2\left(\frac{1}{RT}\right)^3 \frac{\sigma^2 M_{org}^2}{\varepsilon_{org}\upsilon_{org}\rho_{org}\omega^2}$
ω	$\Phi_\omega = \frac{512}{27}\left(\frac{M_w}{\rho_w}\right)^2\left(\frac{1}{RT}\right)^3 \frac{\sigma^3 M_{org}^2}{\varepsilon_{org}\upsilon_{org}\rho_{org}\omega^3}$
υ_{org}	$\Phi_{\upsilon_{org}} = \frac{256}{27}\left(\frac{M_w}{\rho_w}\right)^2\left(\frac{1}{RT}\right)^3 \frac{\sigma^3 M_{org}^2}{\varepsilon_{org}\rho_{org}\upsilon_{org}^2\omega^2} + \frac{M_{org}^2}{\varepsilon_{org}\rho_{org}\upsilon_{org}^2}\left(\sum_{inorg}\left(\frac{\rho_{inorg}}{M_{inorg}}\right)\varepsilon_{inorg}\upsilon_{inorg}\right)$
υ_{org} [a]	$\Phi_{\upsilon_{inorg}} = \left(\frac{\rho_{inorg}}{M_{inorg}}\right)\frac{\varepsilon_{inorg}M_{org}^2}{\varepsilon_{org}\rho_{org}\upsilon_{org}}$
ε_{org}	$\Phi_{\varepsilon_{org}} = \frac{256}{27}\left(\frac{M_w}{\rho_w}\right)^2\left(\frac{1}{RT}\right)^3 \frac{\sigma^3 M_{org}^2}{\upsilon_{org}\rho_{org}\varepsilon_{org}^2\omega^2} + \frac{M_{org}^2}{\upsilon_{org}\rho_{org}\varepsilon_{org}^2}\left(\sum_{inorg}\left(\frac{\rho_{inorg}}{M_{inorg}}\right)\varepsilon_{inorg}\upsilon_{inorg}\right)$
ε_{inorg} [a]	$\Phi_{\varepsilon_{inorg}} = \left(\frac{\rho_{inorg}}{M_{inorg}}\right)\frac{\upsilon_{inorg}M_{org}^2}{\varepsilon_{org}\upsilon_{org}\rho_{org}}$

[a]Inorganics potentially present at T0 are: Na_2SO_4, $NaHSO_4$, $(NH_4)_2SO_4$, NH_4HSO_4, $(NH_4)_3H(SO_4)_2$, $CaSO_4$, K_2SO_4, $KHSO_4$, and $H2SO_4$. Inorganics potentially present at T1 are: $(NH_4)_2SO_4$, NH_4NO_3, NH_4Cl, $CaSO_4$, $Ca(NO_3)_2$, $CaCl_2$, Na_2CO_3, $CaCO_3$, K_2CO_3, Na_2SO_4, and K_2SO_4.

Table 6. Constants From Fitting the Surface Tension Measurements of Pure and Salted Filter Extracts to the Szyskowski-Langmuir Equation[a]

Sample Name (C_{WSOC}[b])	Mixture With $(NH_4)_2SO_4$, f	C_{SO4} (ppm)	$\alpha \times 10^1$ (mN m^{-1}K^{-1})	$\beta \times 10^5$ (ppm^{-1})	Surface Tension Depression[c] (%)
MEX-T0-1 (1030 ppm)	0	1320	8.22	6.35	21.93
	1.333	2956	2.29	24.7	21.91
	12	15060	2.64	22.9	23.59
MEX-T0-2 (995 ppm)	0	1066	6.39	6.68	17.91
	1.333	2629	3.99	11.8	19.29
	12	14188	3.38	14.8	20.22
MEX-T0-4 (896 ppm)	0	654	5.18	4.97	10.89
	1.333	1999	2.93	8.27	10.09
	12	12322	6.28	4.90	13.02
MEX-T0-5 (604 ppm)	0	342	5.84	5.43	13.38
	1.333	996	4.95	5.70	11.89
	12	8120	2.98	11.6	14.18
MEX-T1-1 (578 ppm)	0	235	3.33	6.92	9.66
	0.870	1071	2.60	8.83	9.54
	7.826	7795	3.34	8.26	11.49
MEX-T1-2 (433 ppm)	0	140	4.74	6.06	12.09
	0.870	467	1.50	16.9	10.15
	7.826	2975	1.51	8.99	5.63
MEX-T1-3 (465 ppm)	0	74	2.32	9.34	8.98
	0.870	765	1.14	19.7	8.89
	7.826	6144	6.00	4.10	10.45
MEX-T1-4 (365 ppm)	0	76	1.47	18.2	10.65
	0.870	621	1.95	9.92	7.99
	7.826	4837	9.24	4.39	17.21
MEX-T1-5 (300 ppm)	0	101	1.44	19.5	11.12
	0.870	538	1.29	13.8	7.23
	7.826	4027	1.28	19.7	9.98
MEX-T1-6 (451 ppm)	0	116	0.037	2400	5.16
	0.870	770	3.60	5.25	7.98
	7.826	6004	0.44	50.9	7.85
MEX-T1-7 (348 ppm)	0	54	3.39	3.40	4.91
	0.870	563	3.93	3.38	5.66
	7.826	4598	5.43	5.23	12.00
MEX-T1-8 (227 ppm)	0	22	5.62	3.89	9.30
	0.870	349	5.80	5.18	12.70
	7.826	3003	3.61	8.46	12.71
MEX-T1-9 (296 ppm)	0	35	4.37	4.22	7.83
	0.870	471	2.09	8.60	7.47
	7.826	3924	3.23	7.04	9.52
MEX-T1-10 (850 ppm)	0	78	14.9	1.85	11.84
	0.870	1314	5.45	5.04	11.62
	7.826	11201	9.09	2.66	10.34
MEX-T1-11 (345 ppm)	0	56	3.58	5.66	8.54
	0.870	565	3.58	7.02	10.53
	7.826	4563	2.58	8.78	9.41
MEX-T1-12 (438 ppm)	0	48	4.46	4.03	7.64
	0.870	702	3.43	4.73	6.87
	7.826	5791	3.51	4.68	6.96

[a]Measurements taken at 298 K. Salted filter extracts are salted with $(NH_4)_2SO_4$.
[b]Measured after concentration of samples in the rotavap.
[c]Surface tension depression relative to water at T = 34°C at a C_{WSOC} = 1000 ppm.

4.3. Average Organic Molecular Weight

[33] KTA is used to infer the average organic molar volume based on equation (3), measured surface tension (Table 6), FCA factor, and chemical composition (Tables 3 and 4). During application of KTA, υ_{org} is assumed ~1. For most of the samples collected at T1, an excess of cations (Ca^{2+}, Na^+, and K^+) was present and correlated with dust; excess Ca^{2+} is assumed bound to CO_3^-, while excess K^+ and Na^+ is associated with resuspension of dry lake bed salt from Lake Texcoco [*Vega et al.*, 2001] (located southwest of the T1 site). Metereological data [*de Foy et al.*, 2008; *Fast et al.*, 2007] support this, since on these dates a high-pressure system present over the Gulf of Mexico caused southwesterly winds over the MC area that favored the transport of salt-rich dust from the dry lake bed to the site. To verify that the composition predicted by ISORROPIA-II is representative of the salt mixture in the filter samples, we compared the predicted hygroscopicity of the inorganic fraction with the measured hygroscopicity of samples with an organic fraction approaching zero. Predicted κ at T1 is in the range of 0.3–0.4 (Table 4), which agrees with the observations (Table 2 and Figure 4).

[34] The organic mass fraction in the T0 site samples was low where KTA is subject to large uncertainty [*Padró et al.*,

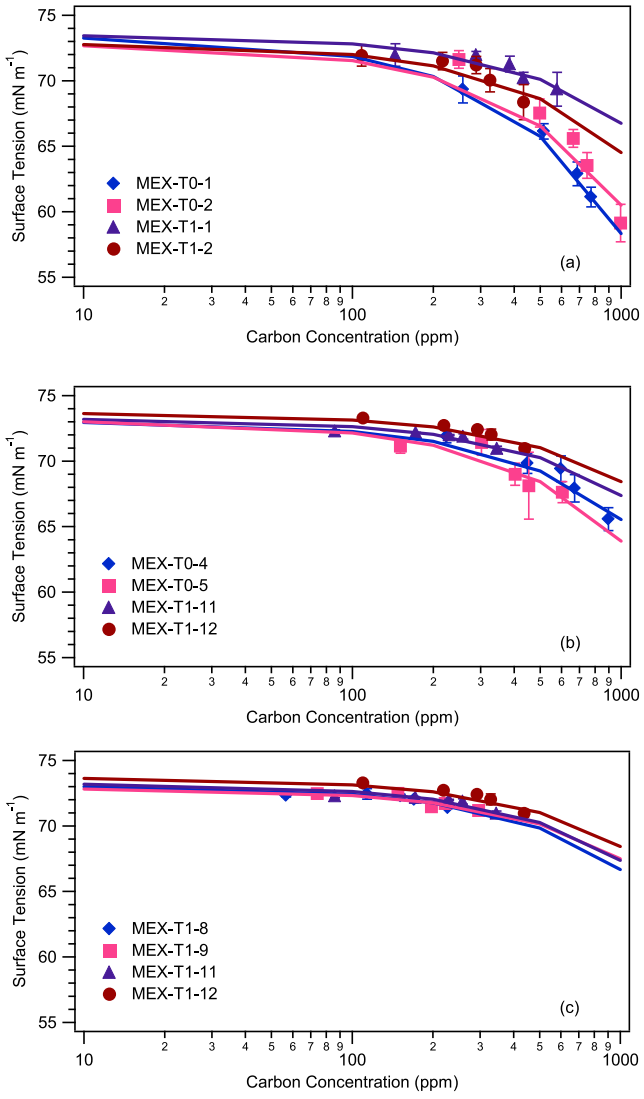

Figure 2. Surface tension as a function of concentration for (a) 24 h integrated samples: MEX-T0-1 (blue diamond), MEX-T0-2 (pink square), MEX-T1-1 (purple triangle), and MEX-T1-2 (maroon circle); (b) 12 h integration day samples: MEX-T0-4 (blue diamond), MEX-T0-5 (pink square), MEX-T1-11 (purple triangle), and MEX-T1-12 (maroon circle); and (c) 12 h integration night samples: MEX-T1-8 (blue diamond), MEX-T1-9 (pink square), and 12 h integration day samples: MEX-T1-11 (purple triangle), and MEX-T1-12 (maroon circle). The solid lines correspond to the Szyskowski-Langmuir fit for each sample.

2007]. Hence molar mass estimates are calculated only for T1 site samples where the organic mass fraction is larger than 50% [*Padró et al.*, 2007] (i.e., all samples except MEX-T1–5 and MEX-T1–7). The molar volumes inferred from KTA when multiplied by the organic density, ρ_{org}, gives an estimation of the organic molecular weight (Table 1). Higher molecular weight organics were found for the 12 h samples (330 amu on average for day and night) relative to the 24 h samples (149 amu on average). The 12 h samples were collected during the third period, which were characterized by high relative humidity and evening rain events, which did not occur in the previous period (before 23 March) [*de Foy et al.*, 2008; *Fast et al.*, 2007]. Under such conditions, the formation of higher molecular weight compounds through condensed-phase chemistry is favored. With the exception of a high O_3 event on 22 March, diurnal changes in gas phase oxidant levels (O_3 and OH) did not vary substantially during the period, hence not likely responsible for this change [*Case Hanks*, 2008]. Increases in sulfur dioxide (SO_2) were however observed from 21–27 March, associ-

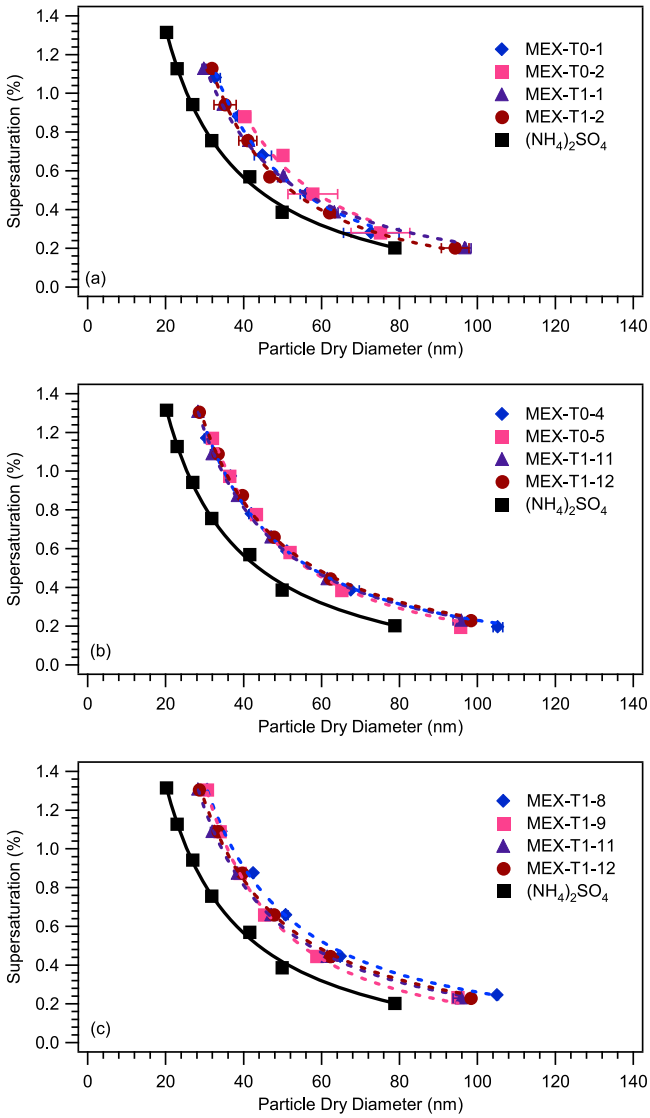

Figure 3. CCN activity for (a) 24 h integrated samples: MEX-T0-1 (blue diamond), MEX-T0-2 (pink square), MEX-T1-1 (purple triangle), and MEX-T1-2 (maroon circle); (b) 12 h integration day samples: MEX-T0-3 (blue diamond), MEX-T0-4 (pink square), MEX-T1-11 (purple triangle), and MEX-T1-12 (maroon circle); and (c) 12 h integration night samples: MEX-T1-8 (blue diamond), MEX-T1-9 (pink square), and 12 h integration day samples: MEX-T1-11 (purple triangle), and MEX-T1-12 (maroon circle) with their corresponding power fit) assuming complete solubility. $(NH_4)_2SO_4$ (black square) is also shown for comparison.

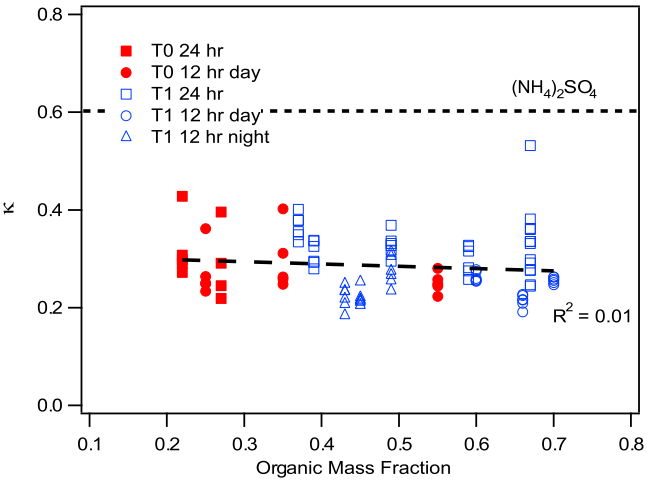

Figure 4. Hygroscopicity parameter versus organic mass fraction: T0 24 h (red square), T0 12 h day (red circle), T1 24 h (blue open square), T1 12 h day (blue open circle), and T1 12 h night (blue open triangle). The black dotted line represents the hygroscopicity parameter for $(NH_4)_2SO_4$.

ated with transport from the Tula power plant [*de Foy et al.*, 2008]; the enhanced RH during this time period, combined with increases in aerosol acidity and sulfate could promote the formation of high molecular weight compounds through a variety of mechanisms, such as acid-catalyzed reactions [e.g., *Jang et al.*, 2002; *Edney et al.*, 2005; *Surratt et al.*, 2007], reactive uptake of volatile aldehydes or ketones via peroxyhemiacetal formation [*Tobias and Ziemann*, 2000; *Docherty et al.*, 2005], hydration, hemiacetal/acetal formation, and aldol condensation [*Jang and Kamens*, 2001; *Jang et al.*, 2002]. For the T1 12 h samples, a lower organic molecular weight (~290 amu on average) was inferred for the day samples (Table 1), consistent with condensation of fresh SOA during peak photochemical activity; subsequent reactions in the condensed phase would tend to increase the average molar mass of the organics at night. This is consistent with oxygenated organic matter dominating the carbonaceous fraction in afternoon and evening periods [*de Gouw et al.*, 2009]. The diurnal profile of size-resolved CCN activity measurements carried out during the same time period [*Lance*, 2007] support this view (although the in situ data exhibit a 30–50% lower κ, likely because not all of the aerosol volume is water-soluble).

4.4. Sensitivity Analysis and Hygroscopicity Parameter Closure

[35] A sensitivity analysis was performed to determine the greatest source of uncertainty in the organic molar mass calculations. Of the six parameters considered (σ, ω, υ_{org}, υ_{inorg}, ε_{org}, and ε_{inorg}), the greatest source of uncertainty arises from the effective van't Hoff factor, followed by the FCA parameter. The total estimated uncertainty in molar mass for all the samples is ~20% (Table 7) similar to levels estimated in other KTA studies [e.g., *Asa-Awuku et al.*, 2008, 2009, 2010; *Engelhart et al.*, 2008; *Moore et al.*, 2008; *Padró et al.*, 2007].

[36] A "κ closure" analysis was also performed to compare the predicted (κ_{mix}) and measured (κ_{CCN}) hygroscopicity parameter values. κ_{CCN} was determined from the s_c and d_{p50} pairs as detailed in section 3.2. κ_{mix} was calculated by applying a mixing rule to the aerosol composition [*Petters and Kreidenweis*, 2007],

$$\kappa_{mix} = \sum_i \varepsilon_i \kappa_i, \tag{7}$$

where κ_i is the hygroscopicity parameter of component i,

$$\kappa_i = \frac{M_w \rho_i \upsilon_i}{\rho_w M_i}. \tag{8}$$

The κ for the water-soluble organic fraction was calculated using the properties determined by KTA (section 4.3). κ for salts potentially present in the extracted filters are presented in Table 2. The κ_{CCN} is sensitive to the assumption of surface tension used (equation (6)), and is evaluated by assuming: (1) the surface tension of water and (2) 15% surface tension from the contribution of organics (an expected value, based on Figures 2a and 2b). It should be pointed out that κ_{mix} is still affected by the surface tension used for calculating M_{org} during application of KTA.

[37] The κ_{mix}-κ_{CCN} closure (Figure 5) shows that neglecting the effects of surface tension depression of organics leads to a 40% underestimation of κ. When κ_{CCN} is calculated allowing for a 15% surface tension depression, excellent closure is obtained between predictions and measurements. This implies that neglecting surfactant char-

Table 7. Molar Mass Uncertainty Analysis and Total Uncertainty as Percent of Molar Mass for the T1 Site Samples

Sample	Uncertainty to σ (g mol^{-1})	Uncertainty to ω (g mol^{-1})	Uncertainty to υ_{org} (g mol^{-1})	Uncertainty to υ_{inorg} (g mol^{-1})	Uncertainty to ε_{org} (g mol^{-1})	Uncertainty to ε_{inorg} (g mol^{-1})	Total Uncertainty (%)
MEX-T1-1	0.105	4.813	15.749	20.892	0.0004	0[a]	14.5
MEX-T1-2	0.047	6.472	3.178	6.674	85.145	0[a]	44.0
MEX-T1-3	0.080	3.740	6.137	17.009	0.001	0[a]	10.8
MEX-T1-4	0.098	7.212	10.057	34.513	0.001	0[a]	22.3
MEX-T1-5	N/A[b]	N/A[b]	N/A[b]	N/A[b]	N/A[b]	N/A[b]	N/A[b]
MEX-T1-6	0.011	0.930	1.032	1.918	0[a]	0[a]	3.3
MEX-T1-7	N/A[b]	N/A[b]	N/A[b]	N/A[b]	N/A[b]	N/A[b]	N/A[b]
MEX-T1-8	0.109	21.291	29.332	96.639	0.001	0[a]	41.4
MEX-T1-9	0.082	15.620	23.676	93.514	0.002	0[a]	28.1
MEX-T1-10	0.045	7.776	16.986	50.696	0.001	0[a]	18.6
MEX-T1-11	0.019	5.316	6.871	19.369	0.001	0[a]	9.97
MEX-T1-12	0.244	5.872	9.498	28.946	0.001	0[a]	10.3

[a]Values are much smaller than 10^{-5} g mol^{-1}.
[b]N/A, not available.

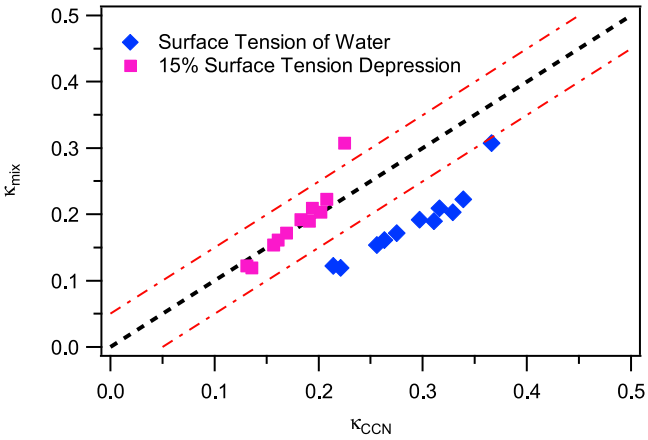

Figure 5. Hygroscopicity parameter closure plot for T1 extracted samples. Comparison of κ_{mix} and κ_{CCN} assuming the surface tension of water (blue diamonds) and 15% surface tension depression (pink squares). The black dashed line represents the 1 to 1 line. The red dash-dotted lines define the 50% error range.

acteristics of the aerosol can result in a substantial overestimation of organic hygroscopicity (even if inorganic salts exist in the particles), which could be important for predictions of CCN concentrations and subsaturated water uptake if substantial amounts of hygroscopic organics are present in the aerosol.

4.5. CCN Activation Kinetics

[38] The impact of water-soluble organics on the CCN activation kinetics was studied using TDGA, which is based on comparing D_w from the sample CCN against that of $(NH_4)_2SO_4$ calibration aerosol. If the droplet sizes from ambient aerosols are smaller than those from calibration aerosol (with same s_c and for identical conditions of instrument operation), the activation kinetics are said to be affected by organics. However, if activated droplet sizes are indistinguishable (to within experimental uncertainty) from $(NH_4)_2SO_4$ data, they are said to exhibit rapid activation kinetics.

[39] Activated droplet sizes obtained for the pure Mexico City samples at both sites (12 h day integration) are shown in Figure 6; droplet sizes are indistinguishable from $(NH_4)_2SO_4$, hence the water-soluble organics present in the Mexico City samples do not retard activation kinetics. However, activation kinetics of in situ CCN performed at T1 can be retarded, particularly during periods of lower hygroscopicity at midday [*Lance*, 2007]. All together, this data suggests that any observed retardations in activation kinetics will be associated with the insoluble fraction. This is consistent with knowledge to date [e.g., *Asa-Awuku et al.*, 2010; *Moore et al.*, 2008; *Engelhart et al.*, 2008; *Sorooshian et al.*, 2008; *Asa-Awuku et al.*, 2009; *Murphy et al.*, 2009; *Bougiatioti et al.*, 2009].

5. Conclusions

[40] Ambient aerosols were collected with Hi-Volume samplers on March 2006 during the MILAGRO field campaign in Mexico City. Particles were collected at the T0 (downtown) and T1 (northeast of the city) sites. Twelve and 24 h filter samples were collected to contrast daytime versus nighttime characteristics. Characterization of the water-soluble fraction was done by measuring its CCN activity, growth kinetics, surface tension, and ionic composition. Köhler Theory Analysis [*Padró et al.*, 2007] was used to infer the average molecular weight of the organics by coupling it to parameters obtained from the offline analysis methods employed here. The κ-Köhler theory analysis was also carried out to examine the variability of the soluble mass hygroscopicity and its sensitivity to the surfactant characteristics of the particulate matter.

[41] From our analysis, we found the water-soluble organics present in Mexico City act as surfactants; surface tension depression was stronger at T0 than at T1, possibly due to more hydrophobic organics present in the former (fresh emissions), further promoted by higher salt concentrations. The most unexpected result is that the water-soluble fraction, regardless of sampling site and period, exhibit remarkably similar CCN activity and hygroscopicity. KTA analysis of the samples suggests that the invariance in κ are a result of changes in molar volume being compensated by surface tension depression. The constant value of κ implies that the CCN activity of the parent aerosol depends solely on its soluble fraction (inorganic and organic combined) and its dry particle diameter. When closure in predicted κ is attempted, neglecting the effects from surfactants may lead to a 50% discrepancy, which is present even if most of the water-soluble fraction is inorganic. Given that this overprediction corresponds to a 15% surface tension depression (which is not atypical for CCN containing surfactants), studies that use a κ-based approach to parameterize compositional impacts on CCN activity need to account for this variability (at least as a sensitivity calculation). Application of KTA to the T1 site samples suggests that the organic molar mass varies between night and day samples by twofold (220 to 430 amu), exhibiting the lowest molar mass during the day. The observed increase in molar

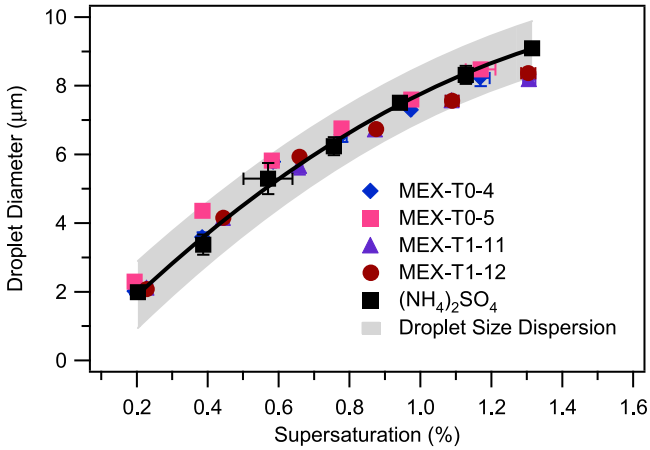

Figure 6. Activated droplet sizes for particles of dry diameter equal to d_{p50}. Results shown for aerosol collected from 12 h integration day samples: MEX-T0-4 (blue diamond), MEX-T0-5 (pink square), MEX-T1-11 (purple triangle), MEX-T1-12 (maroon circle), and $(NH_4)_2SO_4$ (black square). Grey area denotes sizing uncertainty for $(NH_4)_2SO_4$.

mass during the nighttime is consistent with local primary emissions condensing upon the particles, combined with aqueous reactions that could form HULIS. Finally, the activation kinetics of CCN formed from the water-soluble material was found to be similar to $(NH_4)_2SO_4$.

[42] In conclusion, this study suggests that the water-soluble fraction of aerosol as complex as that found in Mexico City exhibits constant hygroscopicity, $\kappa = 0.28 \pm 0.06$, over a wide range of organic mass fraction. Köhler theory analysis of the samples suggests that changes in surface tension may compensate for shifts in average molar mass to give the constant hygroscopicity observed, which implies the amount (volume fraction) of soluble material in the parent aerosol is the key composition parameter required for CCN predictions. This finding, if applicable elsewhere, may explain why CCN predictions are often found to be insensitive to assumptions of chemical composition [e.g., *Dusek et al.*, 2006; *Vestin et al.*, 2007], and provides a very simple way to parameterize organic hygroscopicity in atmospheric models (which for WSOC can be described as $\kappa_{org} = 0.28\varepsilon_{WSOC}$). Special care should be given however to surface tension depression from organic surfactants, as its nonlinear dependence with organic fraction may introduce biases in predicted hygroscopicity.

[43] **Acknowledgments.** This research was supported in part by a NSF CAREER, a NOAA ACC, and a NASA ESSF award. This work was partially supported by NSF ATM 0513035. We would like to thank M. Bergin and G. Hagler (Georgia Institute of Technology) for use of their Turbo Siever 900 TOC analyzer and Büchi rotavapor. We also thank A. G. Russell and E. Cobb (Georgia Institute of Technology) for the use of the Dionex Ion Chromatograph for chemical characterization.

References

Aiken, A. C., et al. (2008), O/C and OM/OC ratios of primary, secondary, and ambient organic aerosols with high-resolution-time-of-flight aerosol mass spectrometry, *Environ. Sci. Technol.*, *42*, 4478–4485, doi:10.1021/es703009q.

Andreae, M. O., and P. J. Crutzen (1997), Atmospheric aerosols: Biogeochemical sources and role in atmospheric chemistry, *Science*, *276*, 1052–1058, doi:10.1126/science.276.5315.1052.

Asa-Awuku, A., A. Nenes, A. P. Sullivan, C. Hennigan, and R. J. Weber (2008), Investigation of molar volume and surfactant characteristics of water-soluble organic compounds in biomass burning aerosol, *Atmos. Chem. Phys.*, *8*, 799–812.

Asa-Awuku, A., G. J. Engelhart, B. H. Lee, S. N. Pandis, and A. Nenes (2009), Relating CCN activity, volatility, and droplet growth kinetics of β-caryophyllene secondary organic aerosol, *Atmos. Chem. Phys.*, *9*, 795–812.

Asa-Awuku, A., A. Nenes, S. Gao, R. C. Flagan, and J. H. Seinfeld (2010), Water-soluble SOA from Alkene ozonolysis: Composition and droplet activation kinetics inferences from analysis of CCN activity, *Atmos. Chem. Phys.*, *10*, 1585–1597.

Badger, C. L., I. George, P. T. Griffiths, C. F. Braban, R. A. Cox, and J. P. D. Abbatt (2006), Phase transitions and hygroscopic growth of aerosol particles containing humic acid and mixtures of humic acid and ammonium sulphate, *Atmos. Chem. Phys.*, *6*, 755–768.

Baumann, K., F. Ift, J. Z. Zhao, and W. L. Chameides (2003), Discrete measurements of reactive gases and fine particle mass and composition during the 1999 Atlanta Supersite Experiment, *J. Geophys. Res.*, *108*(D7), 8416, doi:10.1029/2001JD001210.

Bougiatioti, A., C. Fountoukis, N. Kalivitis, S. N. Pandis, A. Nenes, and N. Mihalopoulos (2009), Cloud condensation nuclei measurements in the eastern Mediterranean marine boundary layer: CCN closure and droplet growth kinetics, *Atmos. Chem. Phys.*, *9*, 7053–7066.

Brooks, S. D., P. J. DeMott, and S. M. Kreidenweis (2004), Water uptake by particles containing humic materials and mixtures of humic materials with ammonium sulfate, *Atmos. Environ.*, *38*, 1859–1868, doi:10.1016/j.atmosenv.2004.01.009.

Butler, A. J. (2000), Temporal and spatial analysis of PM2.5 mass and composition in Atlanta, Ph.D. thesis, School of Civ. and Environ. Eng., Ga. Inst. of Technol., Atlanta.

Carrico, C. M., M. D. Petters, S. M. Kreidenweis, J. L. Collett, G. Engling, and W. C. Malm (2008), Aerosol hygroscopicity and cloud droplet activation of extracts of filters from biomass burning experiments, *J. Geophys. Res.*, *113*, D08206, doi:10.1029/2007JD009274.

Case Hanks, A. T. (2008), Formaldehyde instrument development and boundary layer sulfuric acid: Implications for photochemistry, Ph.D. thesis, School of Earth and Atmos. Sci., Ga. Inst. of Technol., Atlanta.

Clegg, S. L., and P. Brimblecombe (1988), Equilibrium partial pressures of strong acids over concentrated saline solutions—I. HNO_3, *Atmos. Environ.*, *22*, 91–100, doi:10.1016/0004-6981(88)90302-2.

Cobb, C. E. (2006), Spatial and temporal variations of PM2.5 mass and composition in Atlanta: ASACA 1999–2006, M.S. thesis, School of Civ. and Environ. Eng., Ga. Inst. of Technol., Atlanta.

Cross, E. S., T. B. Onasch, M. Canagaratna, J. T. Jayne, J. Kimmel, X.-Y. Yu, M. L. Alexander, D. R. Worsnop, and P. Davidovits (2009), Single particle characterization using a light scattering module coupled to a time-of-flight aerosol mass spectrometer, *Atmos. Chem. Phys.*, *9*, 7769–7793.

DeCarlo, P. F., et al. (2008), Fast airborne aerosol size and chemistry measurements with the high resolution aerosol mass spectrometer during the MILAGRO Campaign, *Atmos. Chem. Phys.*, *8*, 4027–4048.

de Foy, B., et al. (2008), Basin-scale wind transport during the MILAGRO field campaign and comparison to climatology using cluster analysis, *Atmos. Chem. Phys.*, *8*, 1209–1224.

de Gouw, J. A., et al. (2009), Emission and chemistry of organic carbon in the gas and aerosol phase at a sub-urban site near Mexico City in March 2006 during the MILAGRO study, *Atmos. Chem. Phys.*, *9*, 3425–3442.

Dinar, E., T. F. Mentel, and Y. Rudich (2006a), The density of humic acids and humic like substances (HULIS) from fresh and aged wood burning and pollution aerosol particles, *Atmos. Chem. Phys.*, *6*, 5213–5224.

Dinar, E., I. Taraniuk, E. R. Graber, S. Katsman, T. Moise, T. Anttila, T. F. Mentel, and Y. Rudich (2006b), Cloud condensation nuclei properties of model and atmospheric HULIS, *Atmos. Chem. Phys.*, *6*, 2465–2482.

Dinar, E., I. Taraniuk, E. R. Graber, T. Anttila, T. F. Mentel, and Y. Rudich (2007), Hygroscopic growth of atmospheric and model humic-like substances, *J. Geophys. Res.*, *112*, D05211, doi:10.1029/2006JD007442.

Docherty, K. S., W. Wu, Y. B. Lim, and P. J. Ziemann (2005), Contributions of organic peroxides to secondary aerosol formed from reactions of monoterpenes with O_3, *Environ. Sci. Technol.*, *39*, 4049–4059, doi:10.1021/es050228s.

Dusek, U., et al. (2006), Size matters more than chemistry for cloud-nucleating ability of aerosol particles, *Science*, *312*, 1375–1378.

Edney, E. O., T. E. Kleindienst, M. Jaoui, M. Lewandowski, J. H. Offenberg, W. Wang, and M. Claeys (2005), Formation of 2-methyl tetrols and 2-methylglyceric acid in secondary organic aerosol from laboratory irradiated isoprene/NO_x/SO_2/air mixtures and their detection in ambient PM2.5 samples collected in the eastern United States, *Atmos. Environ.*, *39*, 5281–5289, doi:10.1016/j.atmosenv.2005.05.031.

Engelhart, G. J., A. Asa-Awuku, A. Nenes, and S. N. Pandis (2008), CCN activity and droplet growth kinetics of fresh and aged monoterpene secondary organic aerosol, *Atmos. Chem. Phys.*, *8*, 3937–3949.

Facchini, M. C., S. Decesari, M. Mircea, S. Fuzzi, and G. Loglio (2000), Surface tension of atmospheric wet aerosol and cloud/fog droplets in relation to their organic carbon content and chemical composition, *Atmos. Environ.*, *34*, 4853–4857, doi:10.1016/S1352-2310(00)00237-5.

Fast, J. D., et al. (2007), A meteorological overview of the MILAGRO field campaigns, *Atmos. Chem. Phys.*, *7*, 2233–2257.

Fountoukis, C., and A. Nenes (2007), ISORROPIA II: A computationally efficient thermodynamic equilibrium model for K^+–Ca^{2+}–Mg^{2+}–$NH4^+$–Na^+–SO_4^{2-}–NO_3^-–Cl^-–H_2O aerosols, *Atmos. Chem. Phys.*, *7*, 4639–4659.

Hagler, G. S. W., M. H. Bergin, E. A. Smith, and J. E. Dibb (2007), A summer time series of particulate carbon in the air and snow at Summit, Greenland, *J. Geophys. Res.*, *112*, D21309, doi:10.1029/2007JD008993.

Hoffer, A., G. Kiss, M. Blazso, and A. Gelencser (2004), Chemical characterization of humic-like substances (HULIS) formed from a lignin-type precursor in model cloud water, *Geophys. Res. Lett.*, *31*, L06115, doi:10.1029/2003GL018962.

Jang, M. S., and R. M. Kamens (2001), Atmospheric secondary aerosol formation by heterogeneous reactions of aldehydes in the presence of a sulfuric acid aerosol catalyst, *Environ. Sci. Technol.*, *35*, 4758–4766, doi:10.1021/es010790s.

Jang, M. S., N. M. Czoschke, S. Lee, and R. M. Kamens (2002), Heterogeneous atmospheric aerosol production by acid-catalyzed particle-phase reactions, *Science*, *298*, 814–817, doi:10.1126/science.1075798.

Jáuregui Ostos, E. (2000), *El Clima de la Ciudad de México*, 131 pp., Inst. de Geogr., Mexico City.

Kiss, G., E. Tombacz, B. Varga, T. Alsberg, and L. Persson (2003), Estimation of the average molecular weight of humic-like substances isolated from fine atmospheric aerosol, *Atmos. Environ.*, *37*, 3783–3794, doi:10.1016/S1352-2310(03)00468-0.

Kiss, G., E. Tombacz, and H. C. Hansson (2005), Surface tension effects of humic-like substances in the aqueous extract of tropospheric fine aerosol, *J. Atmos. Chem.*, *50*(3), 279–294, doi:10.1007/s10874-005-5079-5.

Kleinman, L. I., et al. (2008), The time evolution of aerosol composition over the Mexico City plateau, *Atmos. Chem. Phys.*, *8*, 1559–1575.

Koehler, K. A., S. M. Kreidenweis, P. J. DeMott, M. D. Petters, A. J. Prenni, and C. M. Carrico (2009), Hygroscopicity and cloud droplet activation of mineral dust aerosol, *Geophys. Res. Lett.*, *36*, L08805, doi:10.1029/2009GL037348.

Lance, S. (2007), Quantifying compositional impacts of ambient aerosol on cloud droplet formation, Ph.D. thesis, School of Earth and Atmos. Sci., Ga. Inst. of Technol., Atlanta.

Lance, S., J. Medina, J. N. Smith, and A. Nenes (2006), Mapping the operation of the DMT continuous flow CCN counter, *Aerosol Sci. Technol.*, *40*, 242–254, doi:10.1080/02786820500543290.

Lance, S., et al. (2009), Cloud condensation nuclei activity, closure, and droplet growth kinetics of Houston aerosol during the Gulf of Mexico Atmospheric Composition and Climate Study (GoMACCS), *J. Geophys. Res.*, *114*, D00F15, doi:10.1029/2008JD011699.

Langmuir, I. (1917), The constitution and fundamental properties of solids and liquids. II. Liquids, *J. Am. Chem. Soc.*, *39*, 1848–1906, doi:10.1021/ja02254a006.

Moffet, R. C., B. de Foy, L. T. Molina, M. J. Molina, and A. Prather (2008), Measurement of ambient aerosols in northern Mexico City by single particle mass spectrometry, *Atmos. Chem. Phys.*, *8*, 4499–4516.

Molina, L. T., et al. (2007), Air quality in North America's most populous city—Overview of the MCMA-2003 campaign, *Atmos. Chem. Phys.*, *7*, 2447–2473.

Moore, R. H., E. D. Ingall, A. Sorooshian, and A. Nenes (2008), Molar mass, surface tension, and droplet growth kinetics of marine organics from measurements of CCN activity, *Geophys. Res. Lett.*, *35*, L07801, doi:10.1029/2008GL033350.

Murphy, S. M., et al. (2009), Comprehensive simultaneous shipboard and airborne characterization of exhaust from a modern container ship at sea, *Environ. Sci. Technol.*, *43*, 4626–4640, doi:10.1021/es802413j.

Padró, L. T., R. Morrison, A. Asa-Awuku, and A. Nenes (2007), Inferring thermodynamic properties from CCN activation experiments: Single-component and binary aerosols, *Atmos. Chem. Phys.*, *7*, 5263–5274.

Petters, M. D., and S. M. Kreidenweis (2007), A single parameter representation of hygroscopic growth and cloud condensation nucleus activity, *Atmos. Chem. Phys.*, *7*, 1961–1971.

Pitzer, K. S., and G. Mayorga (1973), Thermodynamics of electrolytes—II. Activity and osmotic coefficients for strong electrolytes with one or both ions univalent, *J. Phys. Chem.*, *77*, 2300–2308, doi:10.1021/j100638a009.

Roberts, G. C., and A. Nenes (2005), A continuous-flow streamwise thermal-gradient CCN chamber for atmospheric measurements, *Aerosol Sci. Technol.*, *39*, 206–221, doi:10.1080/027868290913988.

Rose, D., G. P. Frank, U. Dusek, S. S. Gunthe, M. O. Andreae, and U. Pöschl (2008), Calibration and measurement uncertainties of a continuous-flow cloud condensation nuclei counter (DMT-CCNC): CCN activation of ammonium sulfate and sodium chloride aerosol particles in theory and experiment, *Atmos. Chem. Phys.*, *8*, 1153–1179.

Ruehl, C. R., P. Y. Chuang, and A. Nenes (2008), How quickly do cloud droplets form on atmospheric particles?, *Atmos. Chem. Phys.*, *8*, 1043–1055.

Ruehl, C. R., P. Y. Chuang, and A. Nenes (2009), Distinct CCN activation kinetics above the marine boundary layer along the California coast, *Geophys. Res. Lett.*, *36*, L15814, doi:10.1029/2009GL038839.

Samburova, V., R. Zenobi, and M. Kalberer (2005), Characterization of high molecular weight compounds in urban atmospheric particles, *Atmos. Chem. Phys.*, *5*, 2163–2170.

Shantz, N. C., W. R. Leaitch, L. Phinney, M. Mozurkewich, and D. Toom-Sauntry (2008), The effect of organic compounds on the growth rate of cloud droplets in marine and forest settings, *Atmos. Chem. Phys.*, *8*, 5869–5887.

Sorooshian, A., S. M. Murphy, S. Hersey, H. Gates, L. T. Padro, A. Nenes, F. J. Brechtel, H. Jonsson, R. C. Flagan, and J. H. Seinfeld (2008), Comprehensive airborne characterization of aerosol from a major bovine source, *Atmos. Chem. Phys.*, *8*, 5489–5520.

Spelt, J. K., and D. Li (1996), *Applied Surface Thermodynamics*, Marcel Dekker, New York.

Stone, E. A., D. C. Snyder, R. J. Sheesley, A. P. Sullivan, R. J. Weber, and J. J. Schauer (2008), Source apportionment of fine organic aerosol in Mexico City during the MILAGRO experiment 2006, *Atmos. Chem. Phys.*, *8*, 1249–1259.

Sullivan, A. P., and R. J. Weber (2006), Chemical characterization of the ambient organic aerosol soluble in water: 2. Isolation of acid, neutral, and basic fractions by modified size-exclusion chromatography, *J. Geophys. Res.*, *111*, D05315, doi:10.1029/2005JD006486.

Sullivan, A. P., R. J. Weber, A. L. Clements, J. R. Turner, M. S. Bae, and J. J. Schauer (2004), A method for on-line measurement of water-soluble organic carbon in ambient aerosol particles: Results from an urban site, *Geophys. Res. Lett.*, *31*, L13105, doi:10.1029/2004GL019681.

Surratt, J. D., et al. (2007), Evidence for organosulfates in secondary organic aerosol, *Environ. Sci. Technol.*, *41*, 517–527, doi:10.1021/es062081q.

Svenningsson, B., et al. (2006), Hygroscopic growth and critical supersaturations for mixed aerosol particles of inorganic and organic compounds of atmospheric relevance, *Atmos. Chem. Phys.*, *6*, 1937–1952.

Taraniuk, I., E. R. Graber, A. Kostinski, and Y. Rudich (2007), Surfactant properties of atmospheric and model humic-like substances (HULIS), *Geophys. Res. Lett.*, *34*, L16807, doi:10.1029/2007GL029576.

Tobias, H. J., and P. J. Ziemann (2000), Thermal desorption mass spectrometric analysis of organic aerosol formed from reactions of 1-tetradecene and O_3 in the presence of alcohols and carboxylic acids, *Environ. Sci. Technol.*, *34*, 2105–2115, doi:10.1021/es9907156.

Turpin, B. J., J. J. Huntzicker, and S. V. Hering (1994), Investigation of organic aerosol sampling artifacts in the Los Angeles Basin, *Atmos. Environ.*, *28*, 3061–3071.

Vega, E., V. Mugica, E. Reyes, G. Sánchez, J. C. Chow, and J. G. Watson (2001), Chemical composition of fugitive dust emitters in Mexico City, *Atmos. Environ.*, *35*, 4033–4039, doi:10.1016/S1352-2310(01)00164-9.

Vestin, A., J. Rissler, E. Swietlicki, G. P. Frank, and M. O. Andreae (2007), Cloud-nucleating properties of the Amazonian biomass burning aerosol: Cloud condensation nuclei measurements and modeling, *J. Geophys. Res.*, *112*, D14201, doi:10.1029/2006JD008104.

Wex, H., T. Hennig, I. Salma, R. Ocksay, A. Kiselev, S. Henning, A. Massling, A. Wiedensohler, and F. Stratmann (2007), Hygroscopic growth and measured and modeled critical supersaturations of an atmospheric HULIS sample, *Geophys. Res. Lett.*, *34*, L02818, doi:10.1029/2006GL028260.

Zappoli, S., et al. (1999), Inorganic, organic and macromolecular components of fine aerosol in different areas of Europe in relation to their water solubility, *Atmos. Environ.*, *33*, 2733–2743, doi:10.1016/S1352-2310(98)00362-8.

C. J. Hennigan and D. Tkacik, Center for Atmospheric Particle Studies, Carnegie Mellon University, Pittsburgh, PA 15213, USA.

G. Huey, T. Lathem, and R. J. Weber, School of Earth and Atmospheric Sciences, Georgia Institute of Technology, 311 Ferst Dr., Atlanta, GA 30332-0340, USA.

A. Nenes and L. T. Padró, School of Chemical and Biomolecular Engineering, Georgia Institute of Technology, 311 Ferst Dr., Atlanta, GA 30332-0340, USA. (athanasios.nenes@gatech.edu)

A. P. Sullivan, Department of Atmospheric Science, Colorado State University, Fort Collins, CO 80523, USA.